QUANTUM-ENHANCED CANCER DETECTION FOR HISTOPATHOLOGIC IMAGES

Nandika Goyal[⋆] *Glen Uehara*[†] *Andreas Spanias*[†]

[⋆] SenSIP Center, School of CAI, Arizona State University, Tempe, AZ, USA
[†] SenSIP Center, School of ECEE, Arizona State University, Tempe, AZ, USA

2025 IEEE International Conference on Image Processing (ICIP) | 979-8-3315-2379-4/25/$31.00 ©2025 IEEE | DOI: 10.1109/ICIP55913.2025.11084595

ABSTRACT

This paper investigates quantum image processing for histopathological cancer detection, focusing on enhanced feature extraction and improved classification. We propose a hybrid quantum-classical framework in which quantum preprocessing circuits, specifically, Quantum Hadamard Edge Detection (QHED) and the Quantum Fourier Transform (QFT), extract subtle spatial and spectral features from hematoxylin and eosin-stained whole-slide images. These quantum-enhanced features are then classified using deep neural networks such as ResNet-50, VGG-16, and UNet. Experiments on the PatchCamelyon dataset demonstrate that quantum-enhanced preprocessing increases sensitivity in detecting cancerous regions, while integrating hybrid preprocessing with an SVM classifier further improves classification accuracy. Although quantum noise remains a challenge, our results highlight the promise of quantum image preprocessing and feature extraction for advancing histopathological image classification.

***Index Terms*—** histopathology images, quantum machine learning, cancer detection, image classification.

1. INTRODUCTION

Cancer remains a leading cause of death globally, with 2.7 million new cases projected by 2030 [1]. Early, accurate detection is critical, motivating the use of quantum computing for histopathology image analysis. Traditional histopathological analysis is invaluable [2] but often time-intensive and reliant on specialized expertise [3]. Pathologists assess features such as cell size, shape, spatial arrangement, and surgical margins [4] to determine cancer presence and progression. However, this manual process can be inefficient and introduce diagnostic uncertainty due to subjectivity [3]. Consequently, there is increasing interest in computer-assisted image analysis to enhance diagnostic precision and consistency [3]. For example, [5] examined cancer type and tumor grade using histopathological examination.

Previous studies have demonstrated the use of deep learning models in automating cancer detection. In [6], deep learning was employed for the evaluation of hepatocellular carcinoma using histopathology images. Ahmad et al. [7] achieved high accuracy with a CNN architecture, and Jaiswal et al. [8] used semi-supervised learning with pre-trained VGG-16 and DenseNet201 models. Furthermore, ensemble approaches by Kassani et al. [9] and Luz et al. [10] yielded promising results on the PCam dataset. Zheng et al. [11] employed AlexNet and ResNet-50 for skin cancer classification, while Bütün et al. [12] used ResNet-101 for lymph node metastasis detection. Yan et al. [13] explored Inception-V3 for breast cancer classification, and Yang et al. [14] showed that ResNet-50 outperformed ResNet-18 for the PathMNIST dataset.

While these classical approaches have yielded promising results, they can fail to capture subtle structural, textural, or spectral nuances—such as early-stage abnormalities or non-local patterns—within high-dimensional histopathology images. Quantum techniques, leveraging superposition and entanglement[15], enable extraction of hidden spatial and frequency-domain features that are often inaccessible to conventional RGB-based analysis[16].a Previous studies [17][18] have shown that hybrid quantum-classical models may improve the speed and accuracy of cancer detection, thereby enabling more effective workflows. Recent studies in quantum machine learning and quantum image processing have further explored hybrid quantum-classical models for medical imaging applications, demonstrating promising results in cancer detection tasks [19][20][21]. While these studies demonstrate the potential of hybrid quantum-classical models, the integration of quantum preprocessing to enhance classical learning architectures for practical clinical workflows remains largely unexplored. Additional work by Majumdar et al. [22] introduced quantum transfer learning for histopathological detection by integrating classical deep learning architectures with variational quantum circuits, achieving classification accuracy comparable to classical models. Azevedo et al. [23] used hybrid quantum machine learning models for breast cancer detection, and Campolongo and Ramachandran [24] implemented a quantum circuit for cancer classification tasks.

Rather than relying solely on quantum kernels, this work explores hybrid fusion models, where **quantum edge detection** (Hadamard + QFT) extracts high-fidelity contour features, and **classical CNNs** (e.g., ResNet-50) or SVMs use these features as input, balancing quantum pattern extraction with deep learning's discriminative power. This design capitalizes on quantum computing's strength in uncovering complex spatial dependencies and the proven accuracy of classical models. Our results demonstrate that this integration not only improves sensitivity in identifying cancerous regions and reduces false negatives but also offers a scalable solution to the limitations of purely classical approaches.

The remainder of this paper is organized as follows: Section II describes the dataset; Section III details the classical algorithms (VGG-16, ResNet-50) and our proposed hybrid quantum-classical methods, including quantum RGB contrast and edge detection circuits for feature extraction. Section IV presents the results, and Section V concludes with key findings and future work.

2. THE PCAM DATASET IMPLEMENTATION CHALLENGES

Standard datasets like MNIST (digits) and CIFAR (color images) are widely used for image recognition, but advanced applications such as medical image analysis require specialized datasets like PatchCamelyon (PCam). PCam comprises 327,680 color images (96×96 pixels) from histopathologic scans of lymph node sections, each labeled for metastatic tissue, making it a binary classification task [25].

In this study, we use the Kaggle version of PCam, modified to remove duplicates from probabilistic sampling [26] (Fig. 1).

Significant implementation challenges arose from the computational demands of quantum image processing. Quantum processing of high-dimensional images (96×96×3) was especially time-consuming, with each image taking 2–10 minutes, depending on circuit complexity, compared to milliseconds for classical methods. All quantum simulations ran locally on an Intel i9-13950HX CPU, 128GB RAM, RTX 3500 GPU, and 2TB NVMe SSD using the Qiskit Aer simulator [27]. Extended training times, spanning days to weeks for both classical and hybrid models, necessitated using reduced dataset portions for some experiments. All quantum circuit measurements were performed using 1024 shots (Qiskit default) to ensure statistical averaging and measurement stability across runs.

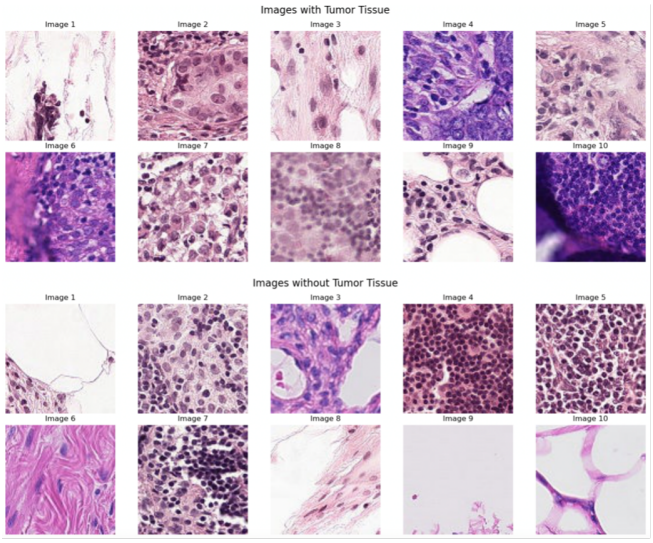

Fig. 1. Cancerous (top) and non-cancerous (bottom) PCam samples.

3. IMAGE CLASSIFICATION ALGORITHMS FOR CANCER DETECTION

Previous studies have examined the strengths and limitations of classical and quantum machine learning (QML) [28] for image classification tasks [29]. Here, we explore how integrating quantum computation with classical models can enhance feature extraction and classification for histopathological cancer detection. We focus on two main approaches: RGB contrast (targeting cell size and shape) and edge detection (emphasizing cell arrangement).

3.1. Classical Benchmarking

The Visual Geometry Group 16 (VGG16) is a widely used deep convolutional neural network with thirteen convolutional and three fully connected layers. Our classical VGG-16 implementation achieved 85.68% accuracy on the full dataset of about 200,000 images.

3.2. RGB Contrast Methods with the VGG-16

3.2.1. Method 1: Quantum Convolution with the VGG-16

We explored quantum convolution by processing 2×2 pixel blocks. Each image I is a 3D tensor $I \in \mathbb{R}^{H \times W \times C}$, where $I_{(h,w,c)}$ denotes the intensity at position (h, w) in channel c. For each 2×2 patch $P_{j,k}$, the pixel intensities are encoded into a quantum state. Specifically, each pixel in the patch corresponds to a qubit, such that a 2×2 block is represented by four qubits. A quantum circuit $U(\varphi)$ is applied, where φ are derived from the pixel intensities of the patch:

$$\varphi = [I_{j,k,0}, I_{j,k+1,0}, I_{j+1,k,0}, I_{j+1,k+1,0}].$$

Here, $I_{j,k,c}$ denotes the intensity at pixel (j, k) for channel c. Each qubit undergoes a rotation $R_Y(\theta)$, where the angle θ is defined as:

$$\theta = \pi \cdot \phi_i, \tag{1}$$

where ϕ_i is the corresponding normalized pixel value for the i-th qubit. The angle θ is derived directly from the input intensities of the 2×2 patch and acts as the input parameter for the rotation gates. The measured values q_0, q_1, q_2, q_3 are used to update the output image.

3.2.2. Method 2: Hybrid Neural Network with the VGG-16

Quantum image processing alone yielded suboptimal performance, so we implemented a hybrid neural network model, combining a classical CNN with a quantum circuit. A feature map encodes the classical input x into a quantum state $|x\rangle$ using a unitary operator with phase shifts and controlled-Z gates to introduce qubit entanglement. Additionally, an ansatz applies parameterized rotations and entangling gates to transform the quantum states.

The quantum neural network (QNN) output is estimated as:

$$\hat{f}(x;\theta) = \langle 0|U^\dagger(\theta)\Phi^\dagger(x)O\Phi(x)U(\theta)|0\rangle, \tag{2}$$

where x is the classical input, θ are the trainable parameters of the quantum circuit $U(\theta)$, $\Phi(x)$ is the feature mapping operator, O is the measurement observable, and † denotes the Hermitian adjoint. While the hybrid model outperformed purely quantum methods, its accuracy remained suboptimal. Therefore, we switched to using ResNet-50 instead of VGG-16 for further experimentation.

3.3. The ResNet-50 Model

The classical ResNet-50 model demonstrated strong performance, achieving high validation accuracy and loss of 15.29% on the full dataset. ResNet-50's deep residual learning architecture allows it to capture complex hierarchical features effectively, making it better suited for histopathological image classification [7][9].

3.4. Method 3: Quantum RGB Contrast Preprocessing with the ResNet-50

We developed a quantum image processing algorithm inspired by the image fusion techniques described by Miller et al. [29]. First, we amplitude encoded the normalized pixel intensities of the image into quantum states, mapping pixel values to the amplitudes of the quantum basis states for subsequent processing. Then, we manipulated the normalized data by passing it through a simple quantum circuit (refer to Fig. 2).

The output binary string updates the four corresponding pixels in the new image matrix I' as follows:

$$I'_{2i,2j} = q_0, \quad I'_{2i,2j+1} = q_1, \quad I'_{2i+1,2j} = q_2, \quad I'_{2i+1,2j+1} = q_3,$$

where q_0, q_1, q_2, q_3 are measurement results from the quantum circuit. The final combined image is computed by:

$$I_{\text{combo}} = \frac{I' + I_{s2r} + I_{s2g} + I_{s2b}}{4}, \tag{3}$$

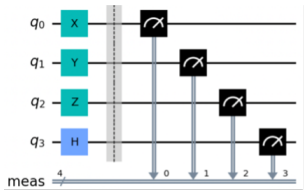

Fig. 2. Proposed quantum circuit for RGB contrast processing.

with $I_{s2r}, I_{s2g}, I_{s2b}$ as the split RGB channels of the original image.

Quantum preprocessing, using the quantum encoding approach with RGB data fusion, resulted in a reduced validation accuracy of 64.86%. Modifying this approach to sum, rather than average, the RGB channels improved accuracy to 76.76% on a subset of the dataset. Both classical and quantum results outperformed other methods. The associated confusion matrices are shown in Fig. 3. The strength of this approach lies in the ability of quantum preprocessing to combine data from multiple channels, enabling improved feature detection through enhanced representation of image information. This method was used in subsequent simulations.

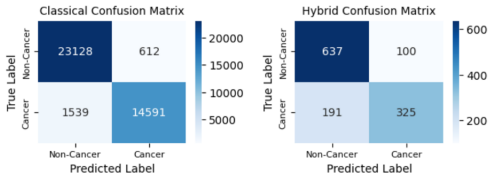

Fig. 3. Confusion matrices: classical ResNet-50 (left) vs. quantum-preprocessed with RGB channel addition ResNet-50 (right).

3.5. Quantum and Classical Edge Detection Techniques

To explore whether edge detection could improve feature extraction, particularly in combination with color analysis, we adapted Rohit Krishna's classical edge detection method [30]. This approach aims to enhance the analysis of cell arrangement and surgical margins, both critical factors in distinguishing cancerous from noncancerous tissue. We began by converting the image to grayscale using a weighted sum of the RGB channels. To reduce noise and prepare the image for edge detection, a Gaussian blur is first applied. The Gaussian kernel is defined as:

$$G(x,y) = \frac{1}{2\pi\sigma^2} \exp\left(-\frac{x^2+y^2}{2\sigma^2}\right), \tag{4}$$

where (x, y) are spatial coordinates relative to the kernel center, and σ controls the spread of the blur.

The smoothed image $I'(x, y)$ is obtained by convolving the original image $I(x, y)$ with the Gaussian filter $G(x, y)$:

$$I'(x,y) = (I * G)(x,y) = \sum_{i=-k}^{k} \sum_{j=-k}^{k} I(x-i, y-j)G(i,j), \tag{5}$$

where k defines the extent of the convolution window around each pixel. Convolution smooths high-frequency variations, enhancing the effectiveness of subsequent gradient-based edge detection methods like the Sobel operator.

Following noise reduction, we used the Sobel operator to compute image gradients and highlight edges. We performed non-maximum suppression to thin the edges, retaining only the local maxima in the direction of the gradient. Double thresholding classified pixels into strong, weak, or non-edges based on two thresholds. Hysteresis was used to track the weak edges connected to strong edges and classify them as strong edges. This method was effective at detecting fine edges and retaining critical structural details, achieving a validation accuracy of 73.33% with ResNet-50 over 10 epochs on approximately 20,000 images.

3.5.1. Method 4: Quantum Edge Detection with the ResNet-50

For quantum Hadamard edge detection, adapted from code by "derivation" [31], images were resized and converted to quantum state vectors. Using Qiskit [27], we designed a quantum circuit (Fig. 4) encoding each pixel intensity as a quantum state:

$$|\psi\rangle = \sum_{i=0}^{N-1} \alpha_i |i\rangle, \quad \text{where} \quad \alpha_i = \frac{\text{PixelIntensity}_i}{\sqrt{\sum_{j=0}^{N-1} (\text{PixelIntensity}_j)^2}}, \tag{6}$$

with N representing the total number of pixels and α_i denoting the normalized amplitude for pixel i.

We then process this state through several key steps:

- **Hadamard Preparation:** Each qubit is placed in an equal superposition, $|0\rangle \xrightarrow{H} (|0\rangle + |1\rangle)/\sqrt{2}$, creating a uniform amplitude distribution across pixel states, which is essential for parallel processing.
- **Entanglement:** Controlled-X gates link pixel qubits, capturing non-local correlations that classical filters cannot.
- **Quantum Fourier Transform (QFT):** Transforms spatial data into the frequency domain,

$$F|x\rangle = \frac{1}{\sqrt{N}} \sum_{k=0}^{N-1} e^{2\pi i x k/N} |k\rangle,$$

  where $|x\rangle$ is the input state and $|k\rangle$ are the Fourier basis states, amplifying high-frequency components (sharp intensity transitions) characteristic of edges.
- **Inverse QFT & Measurement:** IQFT restores spatial information; bit-string measurement reconstructs high-fidelity edge maps.

Edges are detected by analyzing the measured basis states via Qiskit's Statevector Simulator [27]. Combining even and odd detection results yields a complete edge-detected image (see Fig. 5).

Classical filters (Gaussian→Sobel, Canny) apply fixed, linear kernels and lack the ability to capture non-local pixel correlations. By integrating the QFT into a standard Quantum Hadamard Edge Detection (QHED) pipeline, we create a novel enhancement that transitions from spatial domain processing to frequency domain analysis, allowing us to emphasize high-frequency components—i.e., edges. In contrast to classical methods, our quantum circuit's entanglement and QFT/IQFT pipeline enable joint pattern recognition that is classically intractable, yielding richer feature extraction for cancer detection.

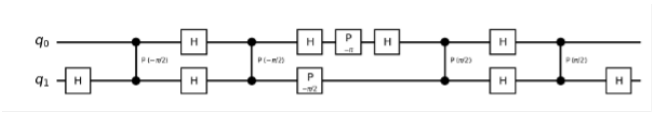

Fig. 4. Quantum edge detection circuit.

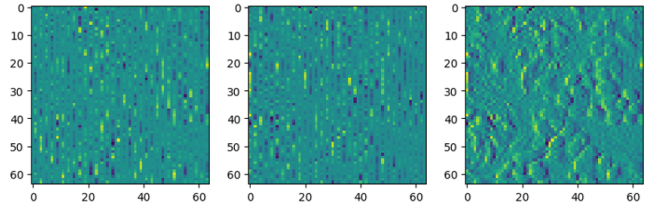

Fig. 5. Even, odd, and combined quantum edge detection results.

3.5.2. Method 5: Hybrid Edge Detection Fusion with the ResNet-50

Experimental results indicated that quantum edge detection alone was ineffective. To enhance performance, we combined the outputs of classical and quantum edge detection. In this fusion approach, the quantum edge map served as a base layer, with classical edges overlaid at 30% transparency (Fig. 6).

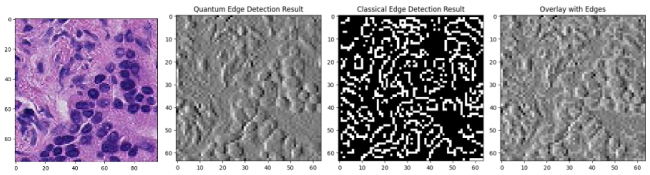

Fig. 6. Original image (left) and result of classical edge detection algorithm, quantum edge detection algorithm, and the fusion with a transparency factor of 30%.

Sensitivity and specificity were calculated for further insight. Sensitivity assesses the test's ability to identify true positives, while specificity assesses true negatives. Combining quantum RGB processing (Method 3) with hybrid edge detection fusion (Method 5) resulted in higher sensitivity than the classical model, indicating an improved ability to detect true positives. However, this increase in sensitivity was accompanied by a noticeable reduction in specificity, suggesting a greater likelihood of false positives. Although the higher sensitivity of the hybrid models results in more false positives, these can be managed through additional testing, which is less concerning compared to the risks associated with false negatives. Therefore, sensitivity was prioritized over specificity in this study to reduce the risk of missing true positives.

3.5.3. Method 6: Hybrid Edge Detection Preprocessing with SVM Classifier

To capitalize on the strengths of both the classical and hybrid models, we implemented a Support Vector Machine (SVM) classifier to combine their predictions. The SVM was trained on predictions from the individual classical and hybrid edge detection fusion models used as input features and the true labels as the target (see Table 1). The results of the classical and hybrid models were averaged over 7 runs, and the SVM Classifier was averaged over 4 runs.

Model	Sens.	Spec.	PPV	NPV	Acc.
Classical ResNet-50	0.6941	0.9453	0.8930	0.8255	0.8460
Hybrid Edge Detection Fusion ResNet-50	0.7460	0.8043	0.7269	0.8220	0.7150
Final SVM Classifier	0.7926	0.8991	...	...	0.8555

Table 1. Comparison of Classical, Hybrid Edge Detection Fusion ResNet-50 Models and Final SVM Classifier Results.

We emphasize that this approach (Fig. 7) successfully leveraged the higher sensitivity of the fusion model and the higher specificity of the classical model, resulting in a balanced classifier that maintains high accuracy by integrating the strengths of both models.

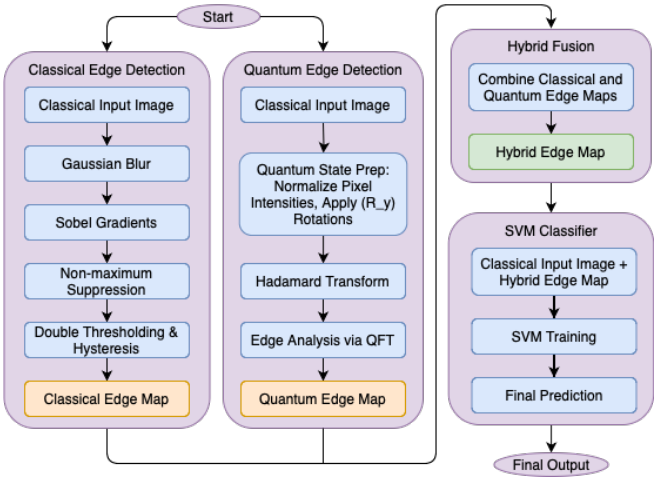

Fig. 7. Workflow of proposed hybrid classical-quantum edge detection framework.

3.6. The UNet Model

We implemented a UNet architecture on the classical and hybrid edge-detected images, modified for classification purposes. The U-Net, a convolutional network architecture originally introduced by Ronneberger et al. [32], is particularly well-suited for biomedical image segmentation tasks where precise localization is crucial, such as in cancer detection. This architecture is notable for its U-shaped structure, which consists of a contracting path (encoder) and an expansive path (decoder). The encoder captures the context of the image by progressively reducing spatial dimensions through downsampling, while the decoder reconstructs the image's spatial resolution to enable precise localization [32]. We modified this architecture for the image classification task by retaining the contracting path but omitting some of the upsampling operations and feature concatenation found in the decoder path. Our implementation produced results consistent with the literature: the classical UNet (Table 2) achieved 83.25% accuracy over 10,000 images and 20 epochs, aligning with the expected 80–85% range and matching classical ResNet performance. The Hybrid Edge Detection UNet showed 7% higher accuracy and 4% higher specificity than the Hybrid Edge Detection ResNet, though with 3% lower sensitivity. In the Quantum RGB Processing (Method 3) + Hybrid Edge Detection Fusion UNet, specificity again exceeded that of its ResNet counterpart, with slightly

lower sensitivity.

Model (Avg over 5 runs)	Sens.	Spec.	PPV	NPV	Acc.
Classical UNet	0.7073	0.9144	0.8443	0.8270	0.8325
Hybrid Edge Detection Fusion UNet	0.7123	0.8405	0.7566	0.8093	0.7881
Quantum RGB + Hybrid Edge Detection UNet	0.6498	0.8684	0.7733	0.7824	0.7791

Table 2. Comparison of Classical and Hybrid Edge Detection Fusion UNets.

4. RESULTS

To isolate each component's contribution, we evaluated the following variants on a 20 k–image subset (averaged over 5–7 runs):

Component	Variants Evaluated
Edge Detection	Quantum (Hadamard + QFT), Classical (Gaussian + Sobel/Canny), None
Encoding Method	Angle encoding, Amplitude encoding, None
Quantum Layer Depth	1-layer QConv, 3-layer QConv
Entanglement Pattern	Linear, Circular, Full
Classical Model	VGG-16 (85.68%), ResNet-50 (84.60%), UNet (83.25%)
Measurement Method	Expectation value, Bit-string probability

Table 3. Ablation study showing components and their evaluated variants across the quantum-classical hybrid pipeline.

Observations & Insights:

- **Edge Detection:** Quantum edge detection yielded the highest sensitivity with ResNet-50.
- **Encoding:** Amplitude encoding preserved relative intensities better but was noisier; angle encoding provided more stable gradients.
- **Layer Depth:** A 1-layer QConv generalized better; 3-layer QConv increased feature richness but risked overfitting.
- **Entanglement Pattern:** Full entanglement boosted nonlocal correlations; linear patterns were more efficient.
- **Model Choice:** ResNet-50 outperformed VGG-16 and UNet on the full dataset; UNet excelled in segmentation tasks.
- **Measurement:** Expectation-value outputs were smoother; bit-string probabilities sharpened binary decisions.

Our final simulations compared classical and hybrid models, as shown in Table 4. The hybrid SVM classifier achieved the strongest overall performance with 85.55% accuracy and 0.7926 sensitivity, representing clear improvements over the classical ResNet-50 baseline. While the hybrid approach reduced specificity from 94.53% to 89.91%, this tradeoff prioritized false negative reduction, which is critical in cancer detection applications where missing malignant regions has severe clinical consequences. The performance improvements stem from the hybrid model's enhanced feature extraction capabilities. Quantum-classical edge detection fusion captures both fine local details and global structural correlations, creating more robust feature representations that simplify SVM decision boundaries and improve feature locality for convolutional models.

Our classical ResNet-50 baseline (84.60% on 10k images) aligns with reported PCam results, where accuracies between 84%–85% were achieved using CNN and semi-supervised models [7][8]. Despite using a smaller training subset, our hybrid SVM fusion reaches 85.55%, demonstrating clear improvement under identical data constraints and reinforcing the efficacy of our hybrid approach.

Model	Sensitivity	Specificity	Accuracy
Classical ResNet-50	0.6941	0.9453	84.60%
SVM Classifier	0.7926	0.8991	85.55%

Table 4. Performance Comparison (10k images)

5. CONCLUSION

This study introduced a unique hybrid classical-quantum preprocessing framework for histopathological cancer detection, integrating quantum computation methods with established classical models to address limitations in traditional medical image analysis approaches. The framework incorporated three key components: quantum edge detection using Hadamard gates and QFT for high-fidelity structural contour capture, RGB Quantum Filtering for quantum-mechanical color encoding, and multi-level fusion strategies combining quantum-encoded features with classical CNN activations (feature-level) and employing voting or ensemble averaging between outputs (decision-level).

Our ablation study revealed critical design insights. Edge detection preprocessing improved performance across all architectures by highlighting structural boundaries and simplifying decision boundaries, particularly benefiting SVMs sensitive to input space geometry [33]. RGB Quantum Filtering captured inter-channel correlations using entanglement and superposition, enriching feature representations beyond classical capabilities. ResNet-50 achieved the highest accuracy through hierarchical feature learning via depth and residual connections, while U-Net excelled in spatial localization with edge-enhanced feature maps.

The hybrid SVM classifier achieved optimal performance with 85.55% accuracy, effectively balancing sensitivity and specificity tradeoffs. The Hadamard + QFT edge extraction pipeline demonstrated a particular advantage in structural contour capture when paired with deep CNNs like ResNet-50. This unique Hadamard + QFT integration demonstrates a promising new direction for quantum-enhanced medical imaging, where the combination of spatial superposition and frequency analysis provides advantages over classical preprocessing methods. These findings demonstrate quantum-enhanced techniques' potential to complement classical computation in high-impact clinical applications where improved sensitivity in detecting true positives is paramount.

Future work will focus on quantum noise reduction and extended training with larger databases. Despite memory constraints necessitating reduced training data in quantum simulations, our hybrid performance approached classical simulations. Enhanced hardware, quantum noise mitigation techniques, and supercomputing cluster access enabling additional training images should enable matching or exceeding classical simulation performance.

6. ACKNOWLEDGMENTS

This project was supported in part by the ASU SenSIP center and industry consortium. Quantum computing tools were also supported by the NSF award 2215998.

7. REFERENCES

[1] S. Lukasiewicz et al., "Breast cancer—epidemiology, risk factors, classification, prognostic markers, and current treatment strategies—an updated review," *Cancers*, vol. 13, no. 17, p. 4287, Aug. 2021.

[2] J. Xie, R. Liu, J. Luttrell, C. Zhang, "Deep learning based analysis of histopathological images of breast cancer," *Frontiers in Genetics*, v. 10, 2019.

[3] W. He et al., "A review: The detection of cancer cells in histopathology based on machine vision," *Computers in Biology and Medicine*, vol. 146, p. 105636, Jul. 2022.

[4] J. Welsh, "What biopsied cancer cells look like under the microscope," https://www.verywellhealth.com/what-cancerlooks-like-5113254.

[5] Chen, X., Liu, X., Wang, L., Zhou, W., Zhang, Y., Tian, Y., Tan, J., Dong, Y., Fu, L. and Wu, H., 2022. Expression of fibroblast activation protein in lung cancer and its correlation with tumor glucose metabolism and histopathology. *European Journal of Nuclear Medicine and Molecular Imaging*, 49(8), pp.2938-2948.

[6] Zhang, X., Yu, X., Liang, W., Zhang, Z., Zhang, S., Xu, L., Zhang, H., Feng, Z., Song, M., Zhang, J. and Feng, S., 2024. Deep learning-based accurate diagnosis and quantitative evaluation of microvascular invasion in hepatocellular carcinoma on whole-slide histopathology images. *Cancer Medicine*, 13(5), p.e7104.

[7] M. Ahmad, I. Ahmed, M. A. Ouameur, G. Jeon, "Classification and detection of cancer in histopathologic scans of lymph node sections using convolutional neural network," *Neur. Proc. Let.*, 55, p. 3763–78, Jul. 2022.

[8] A. K. Jaiswal, I. Panshin, D. Shulkin, N. Aneja, and S. Abramov, "Semi-supervised learning for cancer detection of lymph node metastases," *arXiv preprint arXiv:1906.09587*, Jun. 2019.

[9] S. H. Kassani, P. H. Kassani, M. J. Wesolowski, K. A. Schneider, and R. Deters, Classification of Histopathological Biopsy Images Using Ensemble of Deep Learning Networks, *arXiv preprint arXiv:1909.11870*, Sep. 2019.

[10] D.S. Luz et al, "Automatic detection metastasis in breast histopathological images based on ensemble learning and color adjustment," *Biomedical Signal Processing and Control*, v. 75, p. 103564, May 2022.

[11] Z. Zheng, H. Zhang, X. Li, S. Liu, and Y. Teng, "ResNet-based model for cancer detection," *2021 IEEE ICCECE*, Jan. 2021.

[12] E. Bütün, M. Uçan, and M. Kaya, "Automatic detection of cancer metastasis in lymph node using deep learning," *Biomedical Signal Processing and Control*, vol. 82, p. 104564, Apr. 2023.

[13] R. Yan et al., "Breast cancer histopathological image classification using a hybrid deep neural network," *Methods, Elsevier*, vol. 173, pp. 52–60, Feb. 2020.

[14] J. Yang, R. Shi, B. Ni, "MedMNIST Classification Decathlon: A Lightweight AutoML benchmark for medical image analysis," *2021 IEEE 18th International Symposium on Biomedical Imaging (ISBI)*, Apr. 2021.

[15] J. Preskill, "Quantum Computing in the NISQ era and beyond," *Quantum*, vol. 2, p. 79, Aug. 2018.

[16] P. Rebentrost, M. Mohseni, S. Lloyd, "Quantum Support Vector Machine for Big Data Classification," *Physical Review Letters*, vol. 113, Sep. 2014.

[17] S. Rani, P. Kumar Pareek, J. Kaur, M. Chauhan, and P. Bhambri, "Quantum machine learning in Healthcare: Developments and challenges," *2023 IEEE ICICACS*, Feb. 2023.

[18] M. Rahimi and F. Asadi, "Oncological applications of Quantum Machine Learning," *Technology in Cancer Research & Treatment*, vol. 22, 2023.

[19] D. R. Gonçalves, A. F. Silva, and C. A. Lima, "Quantum Convolutional Neural Networks for Medical Image Classification: A Review and Case Study," *Computers in Biology and Medicine*, vol. 170, p. 107582, 2024.

[20] J. S. Kottmann and A. Aspuru-Guzik, "Variational Quantum Classifiers for Medical Image Analysis," *npj Quantum Information*, vol. 9, no. 1, p. 123, 2023.

[21] G. Mazzola, F. Tacchino, A. Barenco, and D. Gerace, "Quantum Machine Learning for Radiological Image Segmentation," *IEEE Transactions on Medical Imaging*, vol. 42, no. 5, pp. 1175–1185, May 2023.

[22] R. Majumdar, B. Baral, B. Bhalgamiya, and T. D. Roy, Histopathological Cancer Detection Using Hybrid Quantum Computing, *arXiv preprint arXiv:2302.04633*, Feb. 2023.

[23] V. Azevedo, C. Silva, I. Dutra, "Quantum Transfer Learning for Breast Cancer Detection," *Quantum Machine Intelligence*, vol. 4, Feb. 2022.

[24] E. Campolongo and R. SS, "EGRACE479/ERS: QHACK2023 project," https://github.com/egrace479/ERS CRR CT23?tab=readme-ov-file.

[25] Basveeling, "The Patchcamelyon (PCAM) deep learning classification benchmark," GitHub, https://github.com/basveeling/pcam#benchmark.

[26] "Histopathologic Cancer detection," https://www.kaggle.com/competitions/histopathologic-cancer-detection.

[27] A. Javadi-Abhari, M. Treinish, K. Krsulich, C. J. Wood, J. Lishman, J. Gacon, S. Martiel, P. D. Nation, L. S. Bishop, A. W. Cross, B. R. Johnson, and J. M. Gambetta, Quantum computing with Qiskit, *arXiv:2405.08810*.

[28] G. Uehara, A. Spanias, W. Clark, "Quantum Information Processing Algorithms with Emphasis on Machine Learning," *Proc. IEEE IISA 2021*, July 2021.

[29] L. Miller, G. Uehara, and A. Spanias, "Quantum image fusion methods for remote sensing," *2024 IEEE Aerospace Conference*, 70, p. 1–9, Mar. 2024.

[30] R. Krishna, "Canny edge detection algorithm from scratch.," Medium, https://medium.com/@rohit-krishna/coding-canny-edge-detection-algorithm-from-scratch-in-python-232e1fdceac7.

[31] "Quantum Edge Detection," GitHub, https://github.com/derivation/quantum_image_edge_detection/blob/master/detailed_exploration_for_experienced_audience.ipynb.

[32] O. Ronneberger, P. Fischer, T. Brox, "U-Net: Convolutional Networks for Biomedical Image Segmentation," *Lect. Notes in Comp. Sci.*, p. 234, 2015.

[33] K. Muntarina, R. Mostafiz, F. Khanom, S. B. Shorif, and M. S. Uddin, "MultiResEdge: A deep learning-based Edge Detection Approach," *Intelligent Systems with Applications*, vol. 20, p. 200274, Nov. 2023. doi:10.1016/j.iswa.2023.200274